

## Article

# Diurnal Variations and Driving Factors of CO<sub>2</sub> Flux at Water–Air Interfaces in the Open-Flow Sections of Karst Underground Rivers

Danyang Li <sup>1,2,3</sup>, Canfeng Li <sup>1,3</sup>, Chao Huang <sup>1,3</sup>, Hong Li <sup>1,3</sup>, Xiongwei Xu <sup>1,3</sup>, Xuefeng Peng <sup>1,3</sup>, Guiren Chen <sup>1,3</sup> and Liankai Zhang <sup>1,3,\*</sup>

<sup>1</sup> Kunming General Survey of Natural Resources Center, China Geological Survey, Kunming 650100, China; 15512977611@163.com (D.L.); licanfeng@mail.cgs.gov.cn (C.L.); huangchao01@mail.cgs.gov.cn (C.H.); lhong01@mail.cgs.gov.cn (H.L.); xuxiongwei0601@163.com (X.X.); 18313737385@139.com (X.P.); chenguiren@mail.cgs.gov.cn (G.C.)

<sup>2</sup> Chinese Academy of Geological Sciences, China University of Geosciences (Beijing), Beijing 100083, China

<sup>3</sup> Technology Innovation Center for Natural Ecosystem Carbon Sink, Ministry of Natural Resources, Kunming 650100, China

\* Correspondence: zhang\_liankai@126.com

**Abstract:** The high-intensity partial pressure of CO<sub>2</sub> ( $p\text{CO}_2$ ) in karst underground rivers rapidly releases in open-flow sections. This is an important process affecting the global karst carbon cycle. This study focuses on the diurnal variation patterns and driving factors of CO<sub>2</sub> exchange flux at the water–air interface in the open-flow sections of typical karst underground rivers in southwestern China. The inorganic carbon in water and water–air interface exchange fluxes are observed. Three representative survey stations, i.e., the outlet of the underground river (Q1), the river sections without submerged plants (H1), and the river sections with submerged plants (H2), are selected to study the CO<sub>2</sub> exchange process and its influencing factors. The results show that the CO<sub>2</sub> release flux at Q1 exhibits high pressure in the daytime and low pressure in the nighttime, while H1 and H2 exhibit the opposite pattern. The photosynthesis of submerged plants significantly inhibits the carbon release flux of the river, and in the river sections where submerged plants are distributed, their biological effects have inhibited approximately 0.131 Tg C/yr of carbon emissions. This study emphasizes the significant contribution of submerged plants in restraining the release of CO<sub>2</sub>, thereby promoting carbon sequestration and storage in karst water systems.

**Keywords:** open-flow section; water–air interface; CO<sub>2</sub> flux; submerged plants; karst; diurnal variation



**Citation:** Li, D.; Li, C.; Huang, C.; Li, H.; Xu, X.; Peng, X.; Chen, G.; Zhang, L. Diurnal Variations and Driving Factors of CO<sub>2</sub> Flux at Water–Air Interfaces in the Open-Flow Sections of Karst Underground Rivers. *Appl. Sci.* **2024**, *14*, 1395. <https://doi.org/10.3390/app14041395>

Academic Editor: Oleg S. Pokrovsky

Received: 17 December 2023

Revised: 25 January 2024

Accepted: 31 January 2024

Published: 8 February 2024



**Copyright:** © 2024 by the authors. Licensee MDPI, Basel, Switzerland. This article is an open access article distributed under the terms and conditions of the Creative Commons Attribution (CC BY) license (<https://creativecommons.org/licenses/by/4.0/>).

## 1. Introduction

Global carbon cycle research is crucial for understanding the fundamental mechanisms underpinning climate change. According to the current global carbon cycle model, there are carbon missing sinks ranging from 8 to 12 × 10<sup>8</sup> t C/a on land [1]. Therefore, reducing the uncertainty of carbon cycle is necessary to predict variations of atmospheric CO<sub>2</sub> concentration accurately in the future. Karst carbon sinks play a significant role in identifying the missing carbon sinks worldwide [2]. Many studies on karst carbon sinks estimated that the karst carbon sink range from 2.2 to 6.08 × 10<sup>8</sup> t C/a worldwide [3,4]. With the changes in the global climate, the karst carbon sinks are anticipated to have greater significance in missing carbon calculation and global carbon cycle understanding [5]. Therefore, it is crucial to undertake an in-depth research on karst carbon sinks and estimate their flux and exchange trends precisely.

Karst carbon sinks have been recognized as a significant course for slowing climate change [6]. Karstification can increase the sink capacity of ecosystems and decrease the release capacity to the atmosphere [7,8]. However, the karst carbon cycle is complex, as it is sensitive to environmental factors. For instance, global warming may alter the hydrological

cycle in karst regions, which inevitably affects the karst carbon cycle by influencing the carbonate rock weathering pace [9–11] and affecting the CO<sub>2</sub> exchange at the water–air interface [12,13]. Under global climate change and ecological restoration, the karst carbon cycle is becoming more and more impacted by climate parameters such as precipitation, evapotranspiration, runoff, and temperature [14,15]. As reported by Zeng et al. [16], the karst carbon cycle is reacting to global climate change in a sensitive and quick manner.

Although inland water bodies only account for 1% of the Earth's surface area, they play an important role in the carbon cycles of various ecosystems [17]. The water–rock interactions can change the chemical compositions and biological activities of water bodies. The chemical weathering and organic decomposition of underground rivers are two vital processes that contribute to the carbon formation [17–19]. The partial pressure of CO<sub>2</sub> ( $p\text{CO}_2$ ) in underground river water is always more than 110 ppm [20]. The karst underground rivers in southwestern China alone total 1620.57 billion m<sup>3</sup>/a [21], which is equal to 16% of the Yangtze River's annual runoff, and it is 2.8 times the Yellow River's annual runoff. The underground river water in karst regions has a  $p\text{CO}_2$  above 680 ppm and peak reach up to 6166 ppm [22]. However, the degassed carbon flux of underground rivers has been found, in certain studies, to be equal to the net carbon accumulation on the continent (2.2 Pg C/yr) [23–26]. Research on the karst carbon cycle has focused on the open-flow sections of karst underground river water, where aquatic organisms absorb or release high-intensity  $p\text{CO}_2$  at a very rapid pace. Rapid CO<sub>2</sub> release or biological absorption has a major influence on the carbon exchange process, particularly for karst groundwater habitats and ecosystems [2,5,27]. Thus, evaluating the resilience of karst carbon sinks requires investigating the CO<sub>2</sub> exchange process at the water–air interfaces in the open-flow portions of karst underground rivers.

The current state of the karst carbon cycle calculation is hindered by numerous ambiguities regarding the migration and transformation processes of carbon in the open-flow sections of karst underground rivers. The research subject for this paper is a typical karst underground river basin in southwest China. The diurnal variation patterns and driving factors of CO<sub>2</sub> respiration fluxes at the water–air interfaces in karst areas are evaluated by monitoring the carbon in water and water–air interface exchange fluxes at the outlets of underground rivers, river sections without submerged plants in underground rivers, and river sections with submerged plants in karst areas. Additionally, by using the end element method, it is possible to increase the accuracy of river CO<sub>2</sub> flux calculations and strengthen the research on karst carbon sinks by examining the proportion of endogenous organic carbon in water bodies that contributes to organic carbon conversion, investigating the carbon in water conversion processes, and further elucidating the factors that control diurnal changes in carbon release in open-flow sections.

## 2. Materials and Methods

### 2.1. Study Area

The Heilongtan Underground River is a typical karst underground river in Jianshui County, in the Yunnan–Guizhou Plateau southeast China (E102.84°~E102.85°, N23.47°~N23.49°) (Figure 1a). The Xiangchong River, a tributary of the Pear River of China (Figure 1b), originates from this location. The underground river empties into a 20 m tall sheer rock that emerges in the vicinity of Baixiang Mountain on Laogou Street. The annual rainfall in this basin region ranges from 800 to 900 mm. The underground river flows through the karst area and has an abundance of water resources. Water-bearing rocks mainly consist of limestone and dolomite. Underground rivers have a documented dry season flow of 425.06 L/s with a notable increase in flow during the rainy season. The study area receives around 2200 h of sunlight each year, providing sufficient energy for the growth of submerged plants. The dissolved water generally flows from east to west due to the blockage of crust rock in the shape of a bush on the old street, exiting into a fountain, and subsequently forming the surface of the river (Figure 1c). The dominant submerged plant species in this river, between H1 and H2, are *Potamogeton crispus* and *Hydrilla verticillata*.

Both banks of the river are solid and stable, and the study region has consistent weather conditions. During the study period, the Trophic Level Index (TLI ( $\Sigma$ )) was monitored to be less than 30, which means a low level of eutrophication. The average water flow velocity was 0.15 m/s. Research has shown that the growth of algae is limited when the water flow rate exceeds 0.10 m/s, leading to a sharp decrease in cell abundance [28]. Therefore, primary photosynthesis is carried out by submerged plants from the H1 to H2 sections (Figure 1c,d).

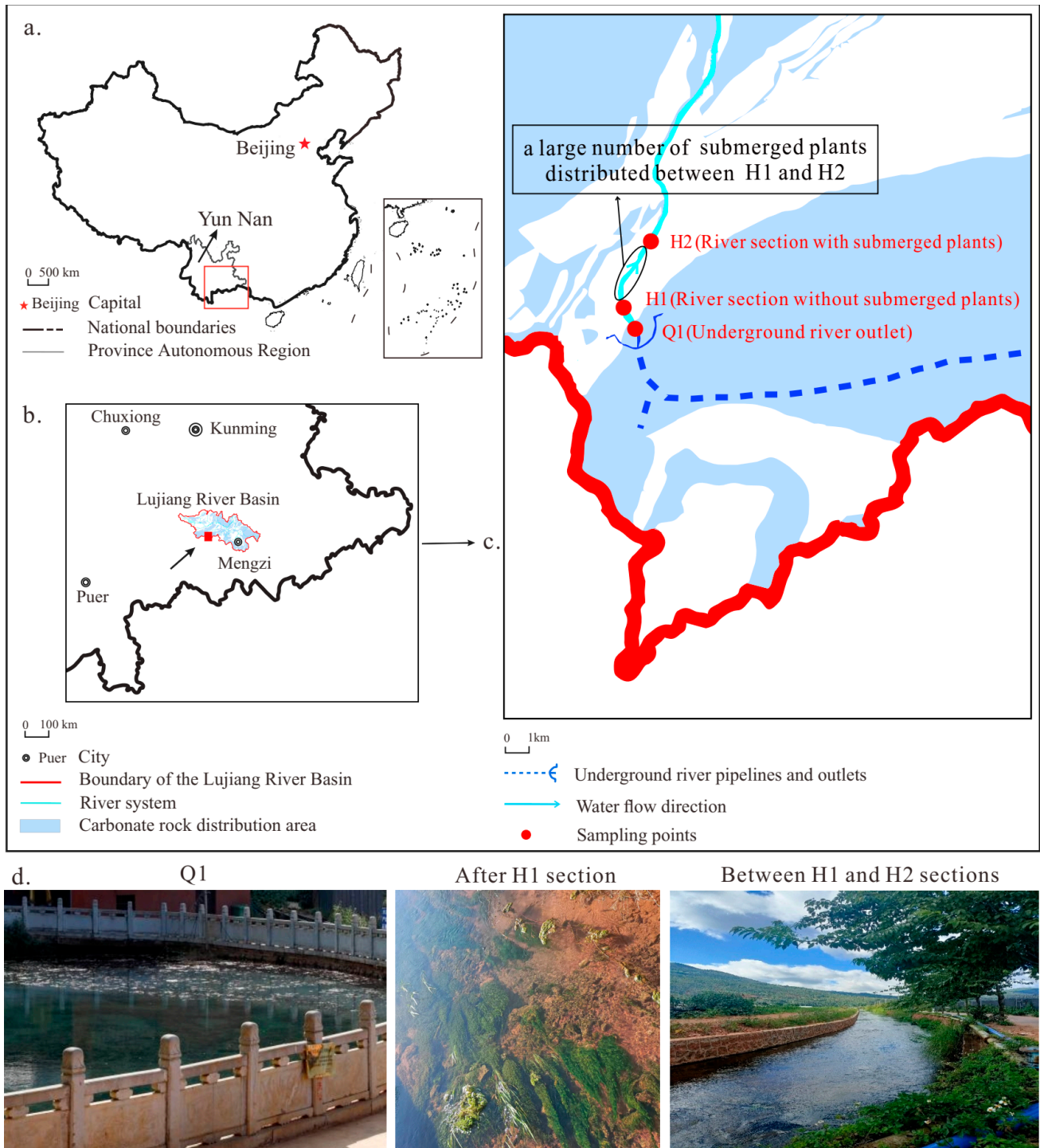


**Figure 1.** Study area location and overview of the sampling points. (a) The relative position of the Lujiang River Basin, (b) the relative position of Heilongtan, (c) monitoring points, (d) specific situation of each monitoring point.

In this study area, the rainy season typically lasts from May to October, and the weather in 2023 is comparatively dry. The rainy season is expected to shift to mid-June. The average water depth during the observation period was 21 cm. The Xiangchong River is a natural waterway with fine sediment, and it serves as an irrigation source for around 20,000 acres in the region of Nanzhuang Town in Jianshui County. The Heilongtan Underground River is mainly used for irrigation and drinking water for people and livestock in the area. It is a significant water source, accounting for one-third of the primary water sources for Jianshui city.

## 2.2. Sample Collection and Processing

At the monitoring sites, there are three river sections: the outlet of the underground river (Q1), the sections without submerged plants (H1), and the sections with submerged plants (H2) (Figure 1d). Cloud coverage can have a significant impact on many environmental variables, including temperature and solar radiation [29]. Therefore, this study was conducted in favorable weather conditions, a gentle climate, consistent water flow, and pre-rainy season when water quality is stable. The study involved a three-day and two-night monitoring period from May 24 to 26, 2023, to observe the water's physical and chemical indicators and continuously measure CO<sub>2</sub> gas levels at the water–air interface. At each of the three sites (Q1, H1, and H2), a multiparameter meter (Ultrameter-II (6P), Myron L Company, Hilliard, OH, USA) was used to monitor the T (water temperature), EC (electrical conductivity), Ta (air temperature), and DO (dissolved oxygen) concentration of the river water at 4-h intervals. The specific EC, temperature, pH, and DO were 0.1 °C, 0.01 mg/L, and 1 µs/cm, respectively. River water samples were collected every four hours from these three sites, after which the samples were placed in a 2 L polyethylene bottle. An inductively coupled plasma emission spectrometer (Intrepid II XSP, Thermo Fisher Scientific, Waltham, MA, USA) was used in the laboratory to measure the cations (K<sup>+</sup>, Na<sup>+</sup>, Ca<sup>2+</sup>, and Mg<sup>2+</sup>) in the water samples after acidification with HNO<sub>3</sub><sup>−</sup> to pH < 2. Additionally, ion chromatography (861 advanced compact IC Metrohm, Herisau, Switzerland) was employed to determine the anion content (F<sup>−</sup>, Cl<sup>−</sup>, NO<sub>3</sub><sup>−</sup>, and SO<sub>4</sub><sup>2−</sup>). The sulfur content and total alkalinity were measured using the silicon molybdenum yellow colorimetric method [30]. The analysis was conducted at the Kunming General Survey of Natural Resources Center, China Geological Survey.

## 2.3. Monitoring of CO<sub>2</sub> Exchange Flux at the Water–Air Interface

In this study, daily variations in greenhouse gas exchange at the water–air interface were measured using a static chamber method. Gas samples were collected every four hours using a flux box made of acrylic board, and a small fan was employed to ensure uniform air mixing inside the box [31]. To isolate the air inside the container from the external environment, the container was set on the water's surface with a floating ring positioned above it [32]. Gas samples were extracted using a syringe and then injected into an aluminum foil storage bag. In the laboratory, gas chromatography was utilized to analyze the CO<sub>2</sub> content with a TDX-01 column used to separate the CO<sub>2</sub> before it was transformed by a methane converter and finally detected using an FID detector.

## 2.4. CO<sub>2</sub> Exchange Flux Calculation

By the following formula [33], the CO<sub>2</sub> exchange flux at the water–gas interface can be determined by monitoring the rate of change in the gas sample concentration:

$$F = \frac{F_1 \times F_2 \times V \times \Delta c}{F_3 \times A \times \Delta t} \quad (1)$$

where F is the gas exchange flux (mg·(m<sup>2</sup>·h)<sup>−1</sup>), F<sub>1</sub> is the unit conversion factor of ppm and µg·m<sup>−3</sup>, F<sub>2</sub> is the conversion coefficient between minutes and days, F<sub>3</sub> is the unit conversion factor between µg and mg, V is the volume of air in the buoyancy chamber (m<sup>3</sup>), and A is the surface area of the floating tank above the water (m<sup>2</sup>). The linear slope

( $10^6 \cdot \text{min}^{-1}$ ) of the greenhouse gas concentration over time during the observation period is represented by the value of  $\Delta c / \Delta t$ .  $F > 0$  denotes the release of greenhouse gases into the atmosphere from bodies of water, such as  $\text{CO}_2$ , whereas  $F < 0$  denotes absorption.

### 2.5. Data Analysis

The measured data in this investigation were processed and computed using Excel 2013. MAPGIS 67 software was used to construct a map of the study area. Phreeqc 3.7.3 software was used to calculate the  $p\text{CO}_2$  in river water and the SIc (saturation index of calcite) using a hydrochemical dataset, including pH; water temperature; and concentrations of  $\text{K}^+$ ,  $\text{Na}^+$ ,  $\text{Ca}^{2+}$ ,  $\text{Mg}^{2+}$ ,  $\text{Cl}^-$ ,  $\text{SO}_4^{2-}$ , and  $\text{HCO}_3^-$ . The remaining data were drawn and analyzed by Origin 2022 and SPSS 25.

## 3. Results and Analysis

### 3.1. Characteristics of Hydrochemical Parameters

The hydrochemical parameters (DIC, SIc, DO, pH, T, EC,  $p\text{CO}_2$ , and Ta) of the Q1, H1, and H2 varied throughout the monitoring period (Figure 2). Comparing H1 and H2 to Q1, it is clear that the former stations have larger daily variations. At Q1, there was no notable diurnal fluctuations, with only minor changes in DO and pH, and other metrics showing small variations. The diurnal variation pattern of DO at Q1 was low during the day and high at night, reaching its peak in the early morning and its lowest point in the late afternoon. In contrast to the variations in SIc, pH, DO, and water temperature, the diurnal variation patterns of DIC, EC, and  $p\text{CO}_2$  at H1 and H2 were low during the day and high at night with the highest and lowest values of DIC, SIc, DO, T, and  $p\text{CO}_2$  occurring nearly simultaneously. At H1, the DIC, EC, and  $p\text{CO}_2$  decreased during the day, peaked in the afternoon, and increased in the evening. Before sunrise, the highest values of DIC and  $p\text{CO}_2$  were observed, and the maximum value of EC was observed prior to early morning. On the other hand, SIc, DO, and T increased during the day, peaked at midday, and decreased during the night, reaching their lowest values in the early morning.

### 3.2. DIC Species

Dissolved inorganic carbon (DIC) is the most important component of carbon in water, mainly including  $\text{HCO}_3^-$ ,  $\text{CO}_3^{2-}$ , and dissolved  $\text{CO}_2$ , in which  $\text{HCO}_3^-$  is the main component of DIC [34]. The average value of  $\text{HCO}_3^-$  at Q1 was 280, with a small change in amplitude, similar to the trend of DIC alkalinity (Figures 2 and 3). The average values of  $\text{HCO}_3^-$  at H1 and H2 were 278 and 264, respectively, showing a trend of low at daytime and high at nighttime, similar to the trend of DIC alkalinity (Figures 2 and 3). The concentrations of  $\text{CO}_3^{2-}$  at Q1 were below 5; changes can be ignored below the method's detection limit. Compared with the  $\text{CO}_3^{2-}$  concentration change at H1, there was a significant change in H2, and the  $\text{CO}_3^{2-}$  concentration at H1 only fluctuates slightly during the day. The average dissolved  $\text{CO}_2$  content at Q1 was 2.53, showing significant fluctuations compared to other DIC composition parameters in Q1. The concentration of  $\text{CO}_3^{2-}$  at H2 was mostly less than 0.03 during most time periods, and only a few time periods showed fluctuations below the method's detection limit.

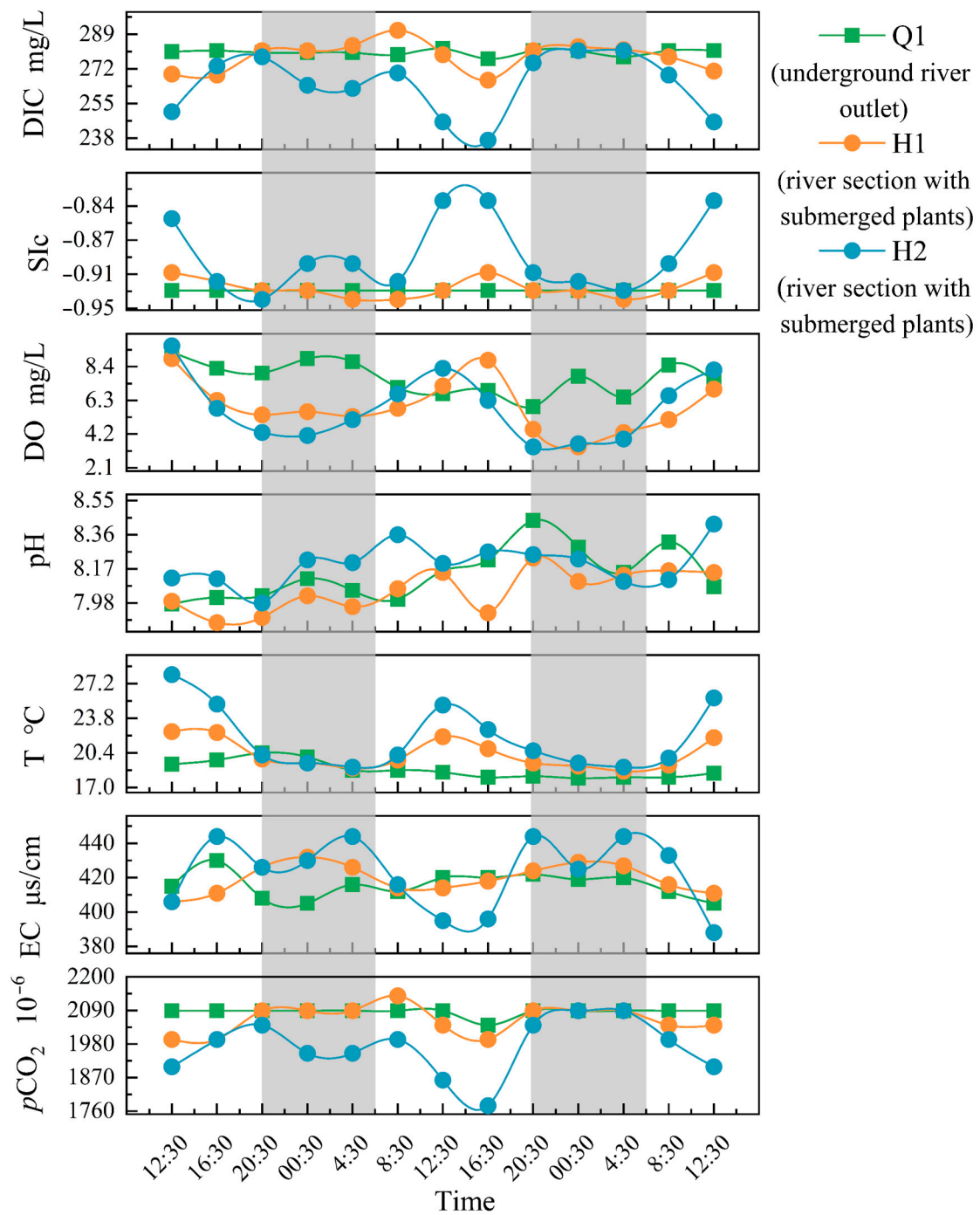


**Figure 2.** The diurnal variation of parameters (note: The gray portion represents the period of night during the sampling period in the study area, while the white portion represents the period of daytime).

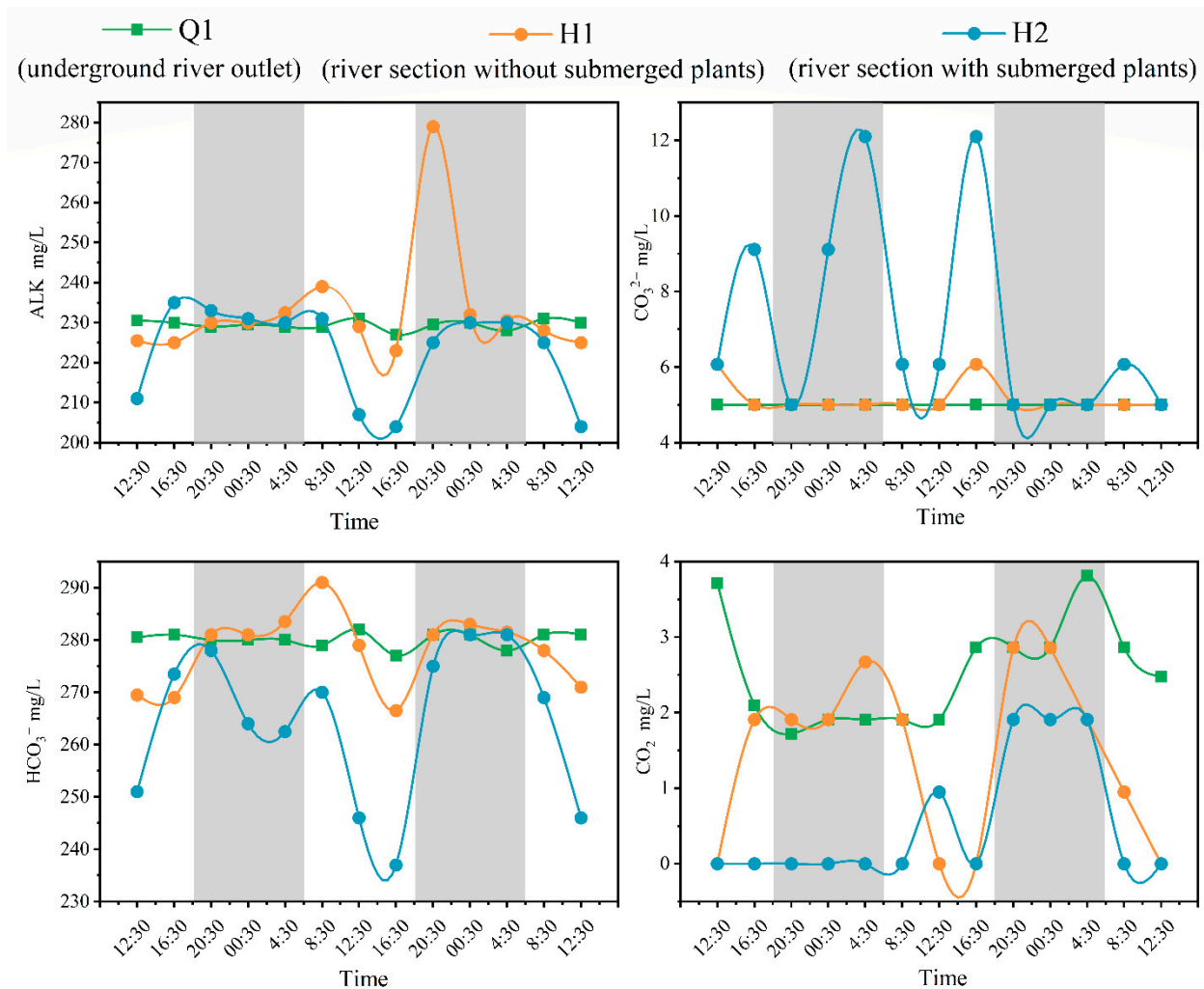


**Figure 3.** Diurnal variation of DIC components in water bodies (note: The gray portion represents the period of night during the sampling period in the study area, while the white portion represents the period of daytime).

### 3.3. CO<sub>2</sub> Fluxes

There was a significant difference ( $p < 0.01$ ) between the average CO<sub>2</sub> exchange flux and the DO concentration at H1 and H2, as shown in Figure 4. The CO<sub>2</sub> exchange flux at H1 ranged from  $-118.49$  to  $116.53$  mmol/(m<sup>2</sup>·d), with fluctuations that caused it to decrease during the day and increase at night. Throughout the entire sampling period, the average CO<sub>2</sub> exchange flux at H1 was  $12.62$  mmol/(m<sup>2</sup>·d), indicating that this section may be a major gas source. The trend of the change in CO<sub>2</sub> exchange flux at Q1 did not show significant fluctuations. The carbon flux calculated during most sampling time periods was positive, and the CO<sub>2</sub> exchange flux at H2 ranged from  $-490.83$  to  $228.34$  mmol/(m<sup>2</sup>·d). The maximum flux appeared in the late afternoon, while the minimum flux was observed in the morning, which is exactly the opposite of the DO. Throughout the sampling period, the average CO<sub>2</sub> exchange flux at H2 was  $-0.68$  mmol/(m<sup>2</sup>·d), indicating that the section may act as a sink for atmospheric CO<sub>2</sub>.

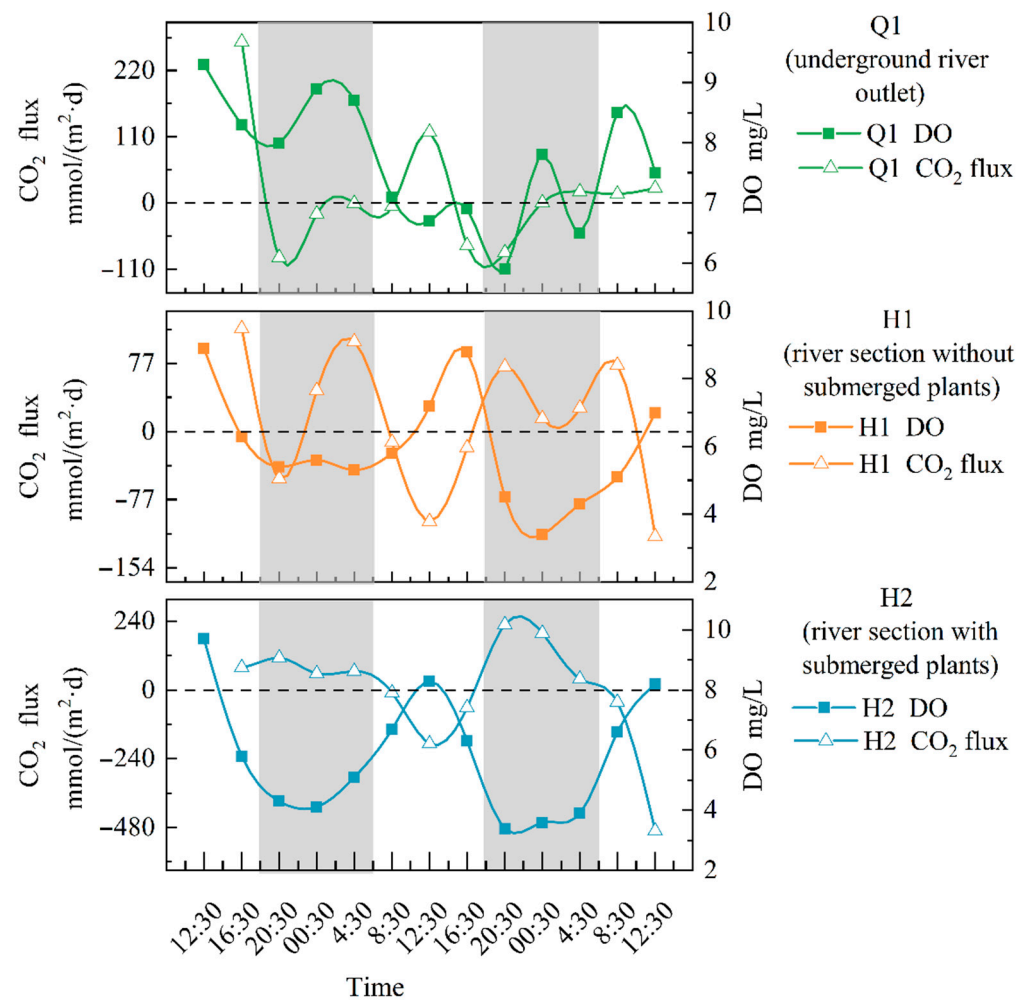


**Figure 4.** Changes in CO<sub>2</sub> flux at different points in the open-flow section (note: The gray portion represents the period of night during the sampling period in the study area, while the white portion represents the period of daytime).

#### 4. Discussion

##### 4.1. The Influence of Factors on CO<sub>2</sub> Exchange Flux

Temperature variations throughout the daytime have an impact on the CO<sub>2</sub> flux [13,19]. At Q1, there is a weak correlation between most parameters with fewer submerged plants and low water flow. The correlation between CO<sub>2</sub> flux and DIC ( $r = 0.41$ ,  $p = 0.19$ ), conductivity ( $r = 0.52$ ,  $p = 0.08$ ), and temperature ( $r = 0.47$ ,  $p = 0.12$ ) is significant and positively correlated. However, the correlation between CO<sub>2</sub> flux and temperature is negative at H1 ( $r = -0.39$ ,  $p = 0.21$ ) and H2 ( $r = -0.59$ ,  $p = 0.04$ ). At Q1, the correlation between air temperature and water temperature is small, while at the river section, there is a strong correlation between air temperature and water temperature. Submerged plants thrive between H1 and H2. The correlation coefficient distribution map (Figure 5) shows that the correlation between various parameters and CO<sub>2</sub> flux is more significant for H2 than for H1, indicating that river submerged plants are closely involved in the process of river carbon absorption and release as well as the alteration of water chemistry and physical indicators.

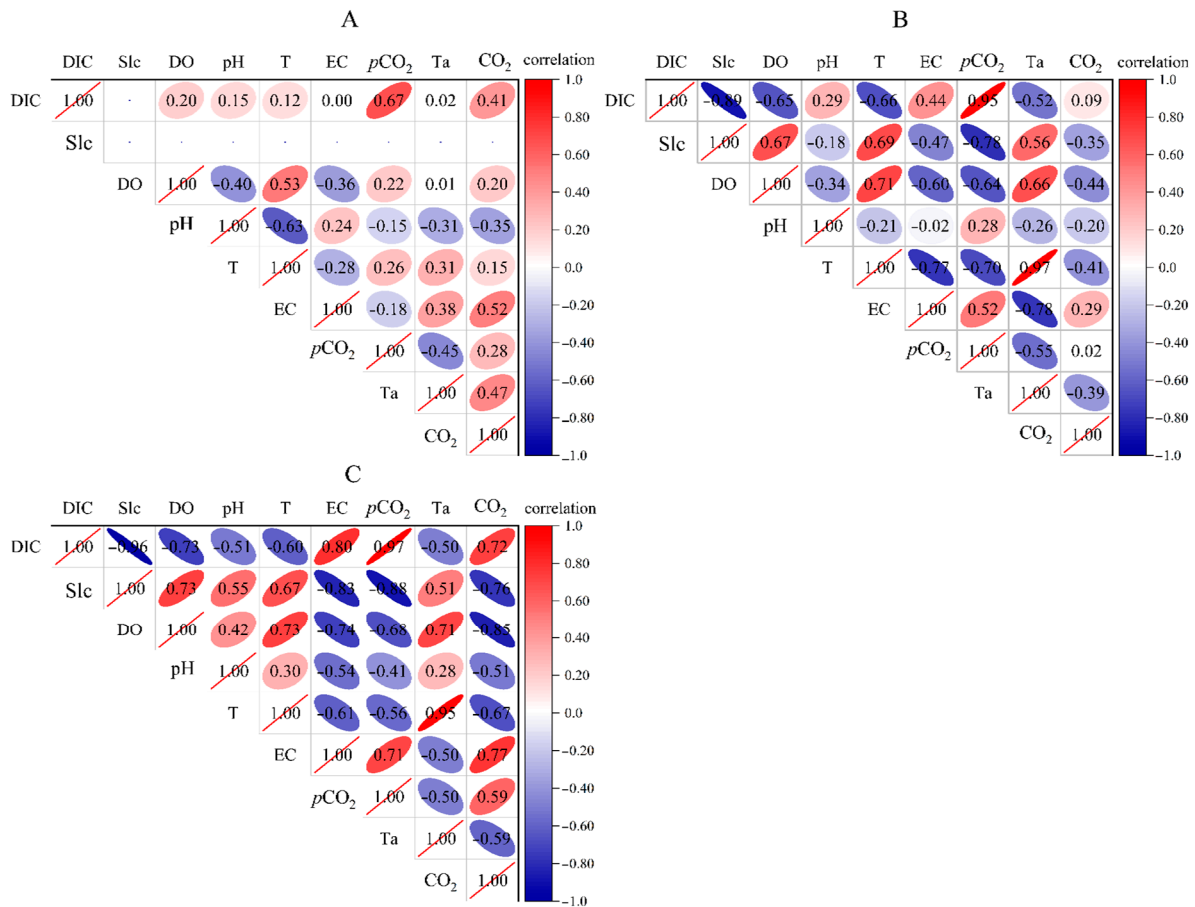


**Figure 5.** Correlation of parameters at different points in the open-flow section (note: 1. (A–C) represent the distribution of correlation coefficients between various parameters at the underground river outlet (Q1), river section without submerged plants (H1), and river section with submerged plants (H2), respectively. 2. The shadow depth in the upper triangle area represents the correlation strength between different elements with red indicating a positive correlation between elements and blue indicating a negative correlation between elements. The darker the color is, the higher the saturation and the more significant the element correlation).

The solubility of CO<sub>2</sub> in water influences the amount of CO<sub>2</sub> released from streams and is negatively correlated to water temperature [33]. The H2 has a higher temperature than the H1, as shown in Figure 2. Theoretically, the CO<sub>2</sub> flux will increase as CO<sub>2</sub> solubility decreases. However, the water temperature is negatively correlated with the CO<sub>2</sub> flux of the H1 ( $r = -0.41, p = 0.18$ ) and H2 ( $r = -0.67, p = 0.02$ ) (Figure 6a), which is consistent with the conclusion from the Lijiang River section [34]. In these two sections, water temperature shows a clear trend of higher temperature during the day and lower temperature at night (similar to the trend of temperature change) (Figure 6b), but the amplitude of change is not significant. Therefore, there are some other processes more influential than temperature in controlling CO<sub>2</sub> release during river flow.

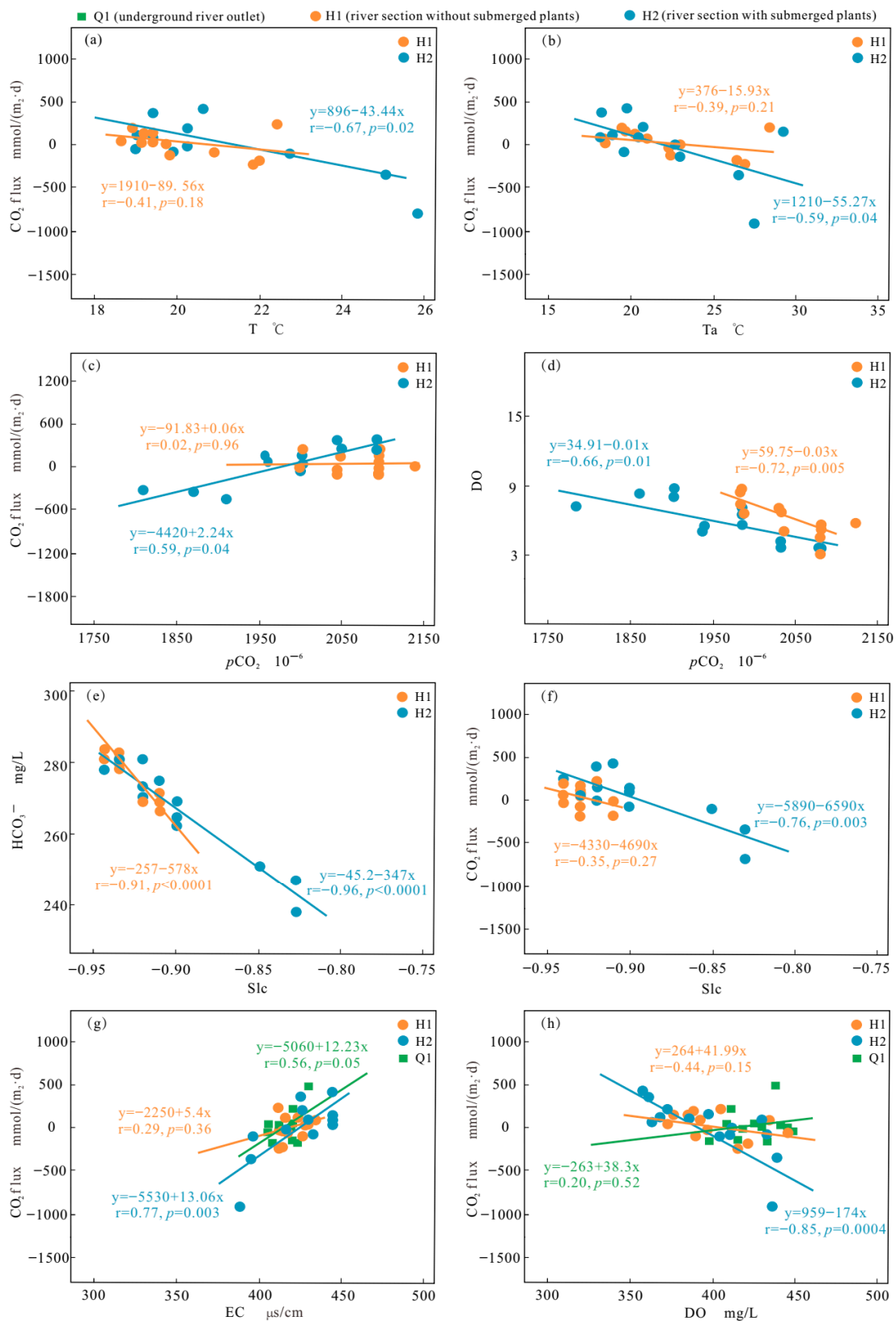


**Figure 6.** Response relationship between CO<sub>2</sub> flux and hydrochemical parameters (note: (a–h) are the results of the fitted line and correlation analysis).

Changes in DO and CO<sub>2</sub> concentrations in river water are directly influenced by the metabolic activities of submerged plants and microbial communities (photosynthesis and

respiration), and variations in  $p\text{CO}_2$  also affect pH levels [35,36]. Changes occurring during the day and night usually lead to periodic diurnal variations in  $\text{CO}_2$  degassing at the water–air interface [37]. Throughout this study, the relationship between  $p\text{CO}_2$  and  $\text{CO}_2$  flux was consistently positive. The study demonstrated an enhanced connection between  $p\text{CO}_2$  and  $\text{CO}_2$  flux at all points (Figure 6c), indicating that metabolic processes largely control  $\text{CO}_2$  release in the Heilongtan River. There was a significant negative correlation between the  $p\text{CO}_2$  concentration and DO concentration (Figure 6d), which reflects the photosynthesis and respiration of submerged plants. An increase in  $p\text{CO}_2$  raises the  $\text{CO}_2$  gradient between the air and water during respiration, leading to increased  $\text{CO}_2$  degassing [27]. Usually,  $\text{CO}_2$  in river water bodies is supersaturated, where the  $p\text{CO}_2$  in rivers is greater than that in the atmosphere [23]. During the day, photosynthesis may exceed respiration, and  $\text{CO}_2$  consumption may cause  $\text{CO}_2$  in the atmosphere to dissolve in river water. The diurnal variation in  $p\text{CO}_2$  at H2 reflects this difference.

The  $p\text{CO}_2$  concentration in rivers is mainly controlled by soil  $\text{CO}_2$  input, the respiration of aquatic microorganisms, and organic matter degradation, which increase  $p\text{CO}_2$ , while the breakdown of carbonate rocks and submerged plant photosynthesis consume  $\text{CO}_2$ , reducing  $p\text{CO}_2$  [38–41]. At Q1, the water had low fluidity, and the lowest  $p\text{CO}_2$  value occurred during the day due to the biological action of microorganisms on the water surface. At H2, the minimum  $p\text{CO}_2$  value during the day was lower than H1, indicating the biological role of submerged plants during water flow.

The influence of carbonate minerals on the concentration of dissolved  $\text{CO}_2$  can be controlled based on the water SIc value [27,42]. A positive SIc value indicates calcite precipitation, which facilitates  $\text{CO}_2$  degassing. Conversely, a negative SIc value indicates calcite dissolution, which restricts  $\text{CO}_2$  escape. During the entire sampling period, the SIc values at all points were  $<0$ , and the H1 ( $r = -0.91$ ,  $p < 0.001$ ) and H2 ( $r = -0.96$ ,  $p < 0.001$ ) and DIC (Figure 6e) showed a substantial negative association, indicating that the dissolution of calcite in the Heilongtan River transformed into  $\text{HCO}_3^-$  in the water, limiting the escape of  $\text{CO}_2$ . However, the various indicator factors of calcite dissolution at Q1 are not correlated, indicating that calcite dissolution does not have a significant impact on the  $\text{CO}_2$  flux changes at the outlet point. There are also other factors that affect the source of  $\text{HCO}_3^-$ : for instance,  $p\text{CO}_2$  ( $r = 0.68$ ,  $p = 0.01$ ). Surprisingly, the SIc values of the H1 ( $r = -0.34$ ,  $p = 0.27$ ) and H2 ( $r = -0.76$ ,  $p < 0.01$ ) show a negative correlation with  $\text{CO}_2$  flux (Figure 6f), which contradicts our theoretical expectations. This indicates that there are other processes that have greater impacts than precipitation or the dissolution of carbonate rocks.

As the conductivity of the water body continuously changes, the  $\text{CO}_2$  flux at Q1, H1, and H2 shows different daily variation patterns. The conductivity is proportional to the total dissolved solids. The conductivity change in section H1 began to show the same change as that of Q1 on the second day, while the conductivity of Q1 was positively correlated with the change in  $\text{CO}_2$  flux ( $r = 0.56$ ,  $p = 0.05$ ) (Figure 6g). The changes in solutes affect the metabolic function of microorganisms in water, which may mainly determine the changes in  $\text{CO}_2$  flux at the H1 section during the flow process. However, during the process from H1 to H2, the dense distribution of submerged plants led to changes in  $\text{CO}_2$  flux at the H2 section. DO ( $p < 0.001$ ) is the primary driver of changes in  $\text{CO}_2$  flux (Figure 6h), while EC ( $p = 0.003$ ) has a significant positive effect (Figure 6g).  $\text{CO}_2$  flux exhibits a diurnal pattern and generally decreases with increasing DO concentration. Therefore, DO is an important variable that may regulate variations in  $\text{CO}_2$  flux.

#### 4.2. Changes in the Sources and Processes of Carbon Components in Rivers

The composition of the basin affects the DIC content of river water, as carbonates and silicates dissolve at different rates [43,44]. In this study,  $\text{HCO}_3^-$  at Q1 mainly originates from carbonate rock weathering, as silicate rock weathering has a negligible impact [45]. DIC mainly includes  $\text{HCO}_3^-$ ,  $\text{CO}_3^{2-}$ , and dissolved  $\text{CO}_2$  [46], with  $\text{HCO}_3^-$  accounting for

approximately 90% of the DIC composition in water. Carbonate rocks are the main source of river DIC in this study area.

The precipitation of carbonate minerals does not always result in the release of CO<sub>2</sub> into the atmosphere, as DIC can be utilized by aquatic photoorganisms to form endogenous organic carbon sinks. Aquatic organisms can transform DIC, POC, DOC, and PIC into each other within the water body [5,26,47]. Photosynthesis increases DO and reduces DIC and HCO<sub>3</sub><sup>−</sup>, while respiration releases CO<sub>2</sub>, increasing DIC and decreasing nighttime DO. There was a positive correlation between DO and HCO<sub>3</sub><sup>−</sup> at H2 ( $r = 0.73, p < 0.01$ ). Changes in DIC are related to pH ( $r = -0.67, p = 0.01$ ) and are not significantly correlated with HCO<sub>3</sub><sup>−</sup> or DO in water. Therefore, changes in DIC are not only related to the photosynthesis of submerged plants but also involve other biological processes.

The organic carbon C/N ratios of the Heilongtan Basin in this study ranged from 6.24 to 10.39 with an average of 8.01. The average organic carbon C/N ratio at the Q1 was 10.39, that at H1 was 7.40, and that at H2 was 6.24. The C/N ratio decreases in the clockwise direction, and the source of TOC is calculated based on the C/N ratio. Previous studies have shown that the C/N ratio of exogenous organic carbon is greater than 15 [48]. According to the typical product of photosynthesis formed by algae, C<sub>5.7</sub>H<sub>9.8</sub>O<sub>2.3</sub>N should have a C/N of 5.7; fungi (C<sub>10</sub>H<sub>17</sub>O<sub>6</sub>N) should have a C/N of 10; and bacteria (C<sub>5</sub>H<sub>7</sub>O<sub>2</sub>N) should have a C/N of 5. Therefore, the C/N ratio of endogenous organic matter should be between 5 and 10. With a C/N ratio of 5.7 as the endogenous endmember and 20.69 as the exogenous endmember [49], the proportion of endogenous organic carbon to total organic carbon can be calculated using a mixed endmember model. The equation is as follows:

$$C/N = f_{au} \times f_B + f_{al} \times (1 - f_B) \quad (2)$$

where C/N is the C/N ratio of the sample;  $f_{au}$  is the endogenous terminal element of the C/N ratio, taken as 5.7;  $f_{al}$  is the external terminal element with a C/N ratio, taken as 20.69; and  $f_B$  is the exogenous organic carbon fraction relative to the total organic carbon.

By combining the concentration values of TOC (POC + DOC) in the Heilongtan Basin, the concentration of endogenous carbon in total organic carbon (TOC<sub>au</sub>) can be calculated, and the equation is as follows:

$$TOC_{au} = TOC \times f_B \quad (3)$$

In the formula, TOC represents the sample's total organic carbon content;  $f_B$  is the endogenous organic carbon fraction relative to the total organic carbon; and TOC<sub>au</sub> is the percentage of total organic carbon that is endogenous carbon.

From Q1 to H1 and H2, the C/N ratio gradually drops as the water flows. The contribution ratios of endogenous organic carbon to TOC are 68.71%, 88.66%, and 96.40%, with an average of 84.59%. The contribution of endogenous organic carbon at Q1 is the least, and the water retention time at Q1 is long. Although there is an absence of submerged plants, the contribution of plankton cannot be ignored. Combining the previous CO<sub>2</sub> flux analysis, it is clear that at Q1, the correlation between the photosynthesis of phytoplankton and CO<sub>2</sub> carbon flux is low, and it may even promote carbon emissions. Moreover, it also indicates that apart from the organic carbon produced by the water's biological carbon pump effect, there is also a 31.29% contribution of exogenous organic carbon at Q1. This is mainly due to Q1 being situated at the outlet of groundwater, where tree leaves on the water surface wither and organic carbon leaches from the upstream soil. The contribution of endogenous organic carbon at H2 is 7.74% higher than H1, and it is close to 1. This indicates that the source of TOC at H2 is mainly organic carbon formed by the biological carbon pump effect, which is a net carbon sink. At the same time, the HCO<sub>3</sub><sup>−</sup> content and DIC value in the water at H2 are lower than those shown for Q1 and H1, and there are a large number of dense submerged plants distributed between H1 and H2, proving that submerged plants utilize DIC in water and convert it into organic carbon (OC). However, it is worth noting that the difference between OC<sub>(H2-H1)</sub> is positive and negative, showing a diurnal trend of positive and negative (Figure 7), indicating that during the day, submerged

plants use DIC as a carbon source for photosynthesis to synthesize OC, and this lifetime yield is greater than the OC consumed by respiration. At night, there is no photosynthesis, and non-autotrophic organisms consume OC, resulting in a decrease in water OC. This consumption rate depends on the type of microorganisms, temperature, and size of organic carbon molecules [50].

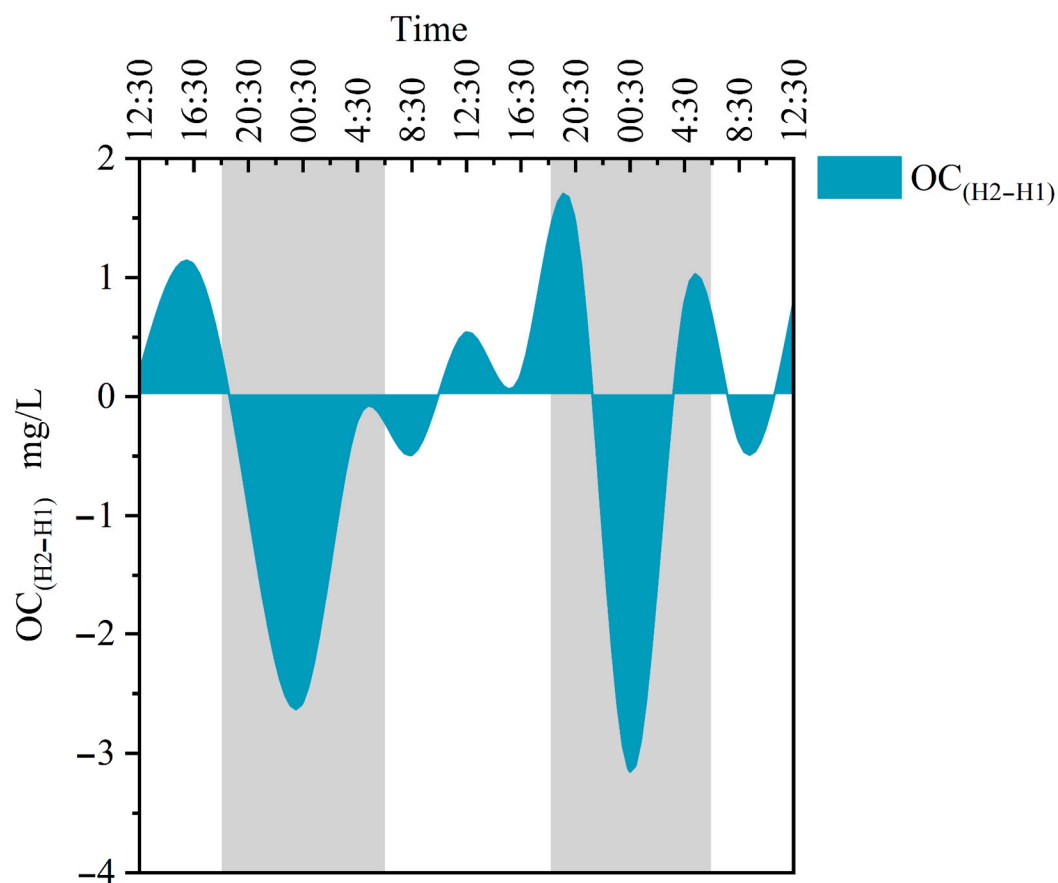


**Figure 7.** Differences in organic carbon changes between H2 and H1. H1 represents the river sections without submerged plants, and H2 represents the river sections with submerged plants. The gray portion represents the period of night during the sampling period in the study area, while the white portion represents the daytime period.

The Beijiang River, Xijiang River and Dongjiang River are the three major tributaries of the Pearl River Basin, each with distinct sources of endogenous organic carbon. The organic carbon C/N ratios of Beijiang, Xijiang, and Dongjiang are 14.44, 15.22, and 9.99, respectively [46]. Calculations show that the contribution sources of endogenous organic carbon in the Beijiang and Xijiang Rivers account for 41.69% and 35.49%, respectively, while the Dongjiang River's contribution is 71.38%. Compared with that in the Pearl River tributary, the contribution of endogenous organic carbon in the Heilongtan River water body was 84.59%, surpassing that of the Dongjiang River, which is largely due to the distribution of submerged plants. The hydraulic conditions of the Heilongtan River in this study area are similar to those of the Dongjiang River: clear water, a gentle riverbed slope, and slow water flow. In addition, a large number of submerged plants are distributed in the water body of the Heilongtan River, which increases the contribution of endogenous organic carbon to the water.

#### 4.3. CO<sub>2</sub> Exchange Flux Comparison of Study Area and the World Rivers

At Q1, H1, and H2, the average CO<sub>2</sub> flux is 14.86 mmol/(m<sup>2</sup>·d), 12.62 mmol/(m<sup>2</sup>·d), and −0.68 mmol/(m<sup>2</sup>·d), respectively. The research results show that the Heilongtan

Basin is an important net flux of CO<sub>2</sub> from rivers to the atmosphere, similar to other major rivers in the world (Table 1). However, in the Heilongtan Basin, CO<sub>2</sub> flux exhibits significant temporal and spatial changes, especially in terms of CO<sub>2</sub> sinks appearing at H2. The average value from H1 to H2 in the Heilongtan Basin is 5.97 mmol/(m<sup>2</sup>·d), which is equivalent to the CO<sub>2</sub> flux of Longchuan (6.87 mmol/(m<sup>2</sup>·d) [51]) but slightly higher than the observed values of other subtropical and tropical rivers [26,52–54]. It is worth noting that the CO<sub>2</sub> flux in the Heilongtan Basin is even lower than in some temperate and northern rivers [55–57]. Research suggests that in Arctic tundra vegetation (moss), metabolic activity exceeds photosynthesis, leading to a significant release of CO<sub>2</sub> [58]. However, this depends on the study area, temperature, and the amount of bicarbonate in the water. In this study area, the release of CO<sub>2</sub> in the open-flow section of karst underground rivers has been reduced due to the biological effects of submerged plants. In inland waters, it has been found that the biological effects of phytoplankton can lead to the release of more CO<sub>2</sub> from the water [59]. Phytoplankton are mostly found in lakes, reservoirs, or slow-moving water bodies, and the CO<sub>2</sub> released from these water bodies is often much greater than that from rivers [32,60]. The CO<sub>2</sub> flux at Q1 is similar to that in reservoirs and may be influenced by phytoplankton. Therefore, the different distribution and geological conditions of submerged plants in water bodies may have a more important impact on CO<sub>2</sub> flux than the climate conditions in the Heilongtan Basin. This further emphasizes the important role of aquatic ecosystems dominated by submerged plants in suppressing CO<sub>2</sub> emissions in karst areas.

**Table 1.** Comparison of CO<sub>2</sub> flux of Heilongtan under different climatic conditions.

Water Type	Name	Country	Climatic Zone	CO <sub>2</sub> Flux/mmol/(m <sup>2</sup> ·d)	Reference
River	Heilongtan H1–H2	China	Subtropic	5.97	This study
	Long Chuan	China	Subtropic	6.87	[51]
	Lower Xljing	China	Subtropic	8.32–15.67	[55]
	Yangtze (Datong)	China	Subtropic	1.69–6.51	[12]
	Hudson	USA	Temperate	0.70–1.63	[26]
	St. Lawrence	Canada	Temperate	1.05–3.62	[61]
	Eastmain, Quebec	Canada	Boreal	0.71	[53]
	Lowet Mekong		Tropic	8.56	[56]
	Amazon	Brazil	Tropic	15.19	[57]
	Tigris	Turkey	Continental	4.74	[54]
York	USA	Warm	1	[62]	
Reservoir	Heilongtan Q1	China	Subtropic	14.86	This study
	Curua–Una	Brazil	Tropic	65.91	[63]
	Tucurui	Brazil	Tropic	192.61	[64]
	Hongfenghu Reservoir	China	Subtropic	20.2	[65]
	Hongjiadu Reservoir	China	Subtropic	6.14	[66]
	Wan’an Reservoir	China	Subtropic	12.74	[60]
	Laforge–1	Canada	Temperate zone	52.27	[33]

The impact of CO<sub>2</sub> balance systems and submerged plant photosynthesis on CO<sub>2</sub> flux are the first two categories of influencing factors for research and analysis. The third category includes the effects of meteorological environmental factors and water-soluble organic and inorganic carbon on CO<sub>2</sub> flux. DO is an important variable that may regulate variations in CO<sub>2</sub> flux. By analyzing the CO<sub>2</sub> flux of the widely distributed river section (from H1 to H2) of submerged plants in the Heilongtan Basin, it was found that the photosynthesis of submerged plants significantly inhibits the carbon flux at H2 with metabolism inhibiting carbon emissions of approximately 0.131 Tg C/yr from H1 to H2. At the same time, it indicates that high-intensity *p*CO<sub>2</sub> is easily absorbed by submerged plants, indicating a process from release to absorption. Therefore, this study emphasizes the process change in CO<sub>2</sub> flux in the open-flow section release to absorption under the metabolism of submerged plants, providing an effective way for carbon sequestration and

sink enhancement in karst water bodies and helping to improve the accuracy of CO<sub>2</sub> flux accounting in rivers.

#### 4.4. The Limitations of Research

This study explores the diurnal variation pattern and driving factors of CO<sub>2</sub> flux at the water–air interface in the open-flow section of a typical karst underground river basin in southwestern China. The study reveals the process of CO<sub>2</sub> flux from release to absorption and evaluates the transformation process of carbon in the river. The study uses the end element mixing model to demonstrate the importance of submerged plants metabolism in the carbon cycle and provides an effective way for carbon sequestration and sink enhancement. However, the study has limitations, including its focus on only one karst underground river basin in southwestern China, the lack of consideration of other factors that may affect the carbon cycle in karst water bodies, and the impact of human activities such as land use change and pollution. Future research could conduct long-term observations of CO<sub>2</sub> flux in different karst underground river basins and study the carbon sequestration effects of submerged plants under different land use types in the open-flow section.

### 5. Conclusions

1. The CO<sub>2</sub> flux in the karst underground river open-flow section of the Heilongtan River shows a pattern of underground river outlet > river sections without submerged plants > river sections with submerged plants (<0). The CO<sub>2</sub> flux at the underground river outlet is high during the day and low at night, while the CO<sub>2</sub> flux in the river sections is low during the day and high at night.

2. The river sections with submerged plants exhibited a substantial correlation ( $p < 0.05$ ) with the CO<sub>2</sub> flux, although the underground river outlet and river sections without submerged plants showed weaker correlations ( $p > 0.05$ ). DO ( $p < 0.001$ ) is an important variable that may regulate variations in CO<sub>2</sub> flux.

3. The end element mixed model calculation shows that at the underground river outlet, river sections without submerged plants, and river sections with submerged plants, the contribution ratio of endogenous organic carbon to TOC is 68.71%, 88.66%, and 96.40%, respectively. This is significantly higher than the ratios found in the Beijiang and Xijiang Rivers of the Pearl River, and it close to the ratio of the Dongjiang River. Combining the distribution of submerged plants with the hydrological circumstances of the Heilongtan and Dongjiang Rivers, it is evident that the metabolism of submerged plants plays a significant regulatory function in the variation of CO<sub>2</sub> flux.

4. The photosynthesis of submerged plants significantly inhibits the carbon flux at the river sections with submerged plants, with metabolism inhibiting carbon emissions of approximately 0.131 Tg C/yr from the river sections without submerged plants to the river sections with submerged plants. In addition, it shows that submerged plants can absorb high-intensity  $p\text{CO}_2$ , suggesting a mechanism that goes from release to absorption.

**Author Contributions:** Conceptualization, D.L. and L.Z.; data curation, D.L., X.P. and C.H.; validation, C.H. and L.Z.; formal analysis, D.L., C.L., H.L. and X.X.; investigation, D.L., L.Z. and G.C.; writing—original draft preparation, D.L.; writing—review and editing, L.Z. and C.L. All authors have read and agreed to the published version of the manuscript.

**Funding:** This research was funded by (Geological Survey Project of China Geological Survey Bureau) grant number (DD20230111, DD20230512).

**Institutional Review Board Statement:** Not applicable.

**Informed Consent Statement:** Not applicable.

**Data Availability Statement:** The data presented in this study are available on request from the corresponding author. The dates are not publicly available due to the privacy of the data.

**Conflicts of Interest:** The authors declare no conflicts of interest.

## References

1. Davies, B.T.; Valdes, P.J.; Singarayer, J.S.; Wiltshire, A.J.; Jones, C.D. Quantifying the relative importance of land cover change from climate and land use in the representative concentration pathways. *Glob. Biogeochem. Cycles* **2019**, *29*, 842–853. [[CrossRef](#)]
2. Liu, Z.H.; Dreybrodt, W. Significance of the carbon sink produced by H<sub>2</sub>O–carbonate–CO<sub>2</sub>–aquatic phototroph interaction on land. *Sci. Bull.* **2015**, *60*, 182–191. [[CrossRef](#)]
3. Yuan, D.X. Sensitivity of karst process to environmental change along the Pep II transect. *Quat. Int.* **1997**, *37*, 105–113. [[CrossRef](#)]
4. Liu, Z.H.; Dreybrodt, W.; Wang, H.J. A potentially important CO<sub>2</sub> sink generated by the global water cycle. *Sci. Bull.* **2007**, *52*, 2418–2422.
5. Liu, Z.; Dreybrodt, W.; Wang, H. A new direction in effective accounting for the atmospheric CO<sub>2</sub> budget: Considering the combined action of carbonate dissolution, the global water cycle and photosynthetic uptake of DIC by aquatic organisms. *Earth Sci. Rev.* **2010**, *99*, 162–172. [[CrossRef](#)]
6. Aufdenkampe, A.K.; Mayorga, E.; Raymond, P.A.; Melack, J.M.; Doney, S.C.; Alin, S.R. Riverine coupling of biogeochemical cycles between land, oceans, and atmosphere. *Front. Ecol. Environ.* **2011**, *9*, 53–60. [[CrossRef](#)]
7. Larson, C. Climate change. An unsung carbon sink. *Science* **2011**, *334*, 886–887. [[CrossRef](#)] [[PubMed](#)]
8. Liu, Z.H.; Dreybrodt, W.; Liu, H. Atmospheric CO<sub>2</sub> sink: Silicate weathering or carbonate weathering? *Appl. Geochem.* **2011**, *26*, 5292–5294. [[CrossRef](#)]
9. Yu, S.; He, S.Y.; Sun, P.A.; Pu, J.B.; Huang, J.; Luo, H.X.; Li, Y.S.; Li, R.; Yuan, Y.Q. Impacts of anthropogenic activities on weathering and carbon fluxes: A case study in the Xijiang River basin, southwest China. *Environ. Earth Sci.* **2016**, *75*, 1–11. [[CrossRef](#)]
10. Atekwana, E.A.; Fonyuy, E.W. Dissolved inorganic carbon concentrations and stable carbon isotope ratios in streams polluted by variable amounts of acid mine drainage. *J. Hydrol.* **2009**, *372*, 136–148. [[CrossRef](#)]
11. Sharma, S.; Sack, A.; Adams, J.P.; Vesper, D.V.; Capo, R.C.; Hartsock, A.; Edenborn, H.M. Isotopic evidence of enhanced carbonate dissolution at a coal mine drainage site in Allegheny County, Pennsylvania, USA. *Appl. Geochem.* **2013**, *29*, 32–42. [[CrossRef](#)]
12. Peter, H.; Singer, G.A.; Preiler, C.; Chiffard, P.; Steniczka, G.; Battin, T.J. Scales and drivers of temporal pCO<sub>2</sub> dynamics in an Alpine stream. *J. Geophys. Res. Biogeosci.* **2014**, *119*, 1078–1091. [[CrossRef](#)]
13. Wang, F.S.; Wang, Y.C.; Zhang, J.; Xu, H.; Wei, X.G. Human impact on the historical change of CO<sub>2</sub> degassing flux in River Changjiang. *Geochem. Trans.* **2007**, *8*, 1–10. [[CrossRef](#)] [[PubMed](#)]
14. Gu, L.; Chen, J.; Yin, J.B.; Xu, C.Y.; Zhou, J.H. Responses of Precipitation and Runoff to Climate Warming and Implications for Future Drought Changes in China. *Earth's Future* **2020**, *8*, 32. [[CrossRef](#)]
15. Gong, S.H.; Wang, S.J.; Bai, X.Y.; Luo, G.J.; Zeng, C. Response of the weathering carbon sink in terrestrial rocks to climate variables and ecological restoration in China. *Sci. Total Environ.* **2020**, *750*, 141525. [[CrossRef](#)] [[PubMed](#)]
16. Zeng, S.B.; Liu, Z.H.; Kaufmann, G. Sensitivity of the global carbonate weathering carbon-sink flux to climate and land-use changes. *Nat. Commun.* **2019**, *10*, 5749. [[CrossRef](#)] [[PubMed](#)]
17. Battin, T.J.; Luysaert, S.; Kaplan, L.A.; Aufdenkampe, A.K.; Richter, A.; Tranvik, L.J. The boundless carbon cycle. *Nat. Geosci.* **2009**, *2*, 598–600. [[CrossRef](#)]
18. Hope, D.; Palmer, S.M.; Billett, M.F.; Dawson, J.J.C. Variations in dissolved CO<sub>2</sub> and CH<sub>4</sub> in a first-order stream and catchment: An investigation of soil–stream linkages. *Hydrol. Process.* **2004**, *18*, 3255–3275. [[CrossRef](#)]
19. Lynch, J.K.; Beatty, C.M.; Seidel, M.P.; Jungst, L.J.; Degrandpre, M.D. Controls of riverine CO<sub>2</sub> over an annual cycle determined using direct, high temporal resolution pCO<sub>2</sub> measurements. *J. Geophys. Res.* **2010**, *115*, 3016. [[CrossRef](#)]
20. Ni, M.F.; Li, S.Y. Partial Pressure of Carbon Dioxide and Water-air Exchange in a Typical Karst River. *Quat. Sci.* **2023**, *43*, 412–424.
21. Cao, J.H.; Jiang, Z.C.; Yuan, D.X.; Xia, R.Y.; Zhang, C. The progress in the study of the karst dynamic system and global changes in the past 30 years. *Geol. China* **2017**, *44*, 874–900. (In Chinese)
22. Zhang, T.; Li, J.H.; Pu, J.B.; Wu, F.H.; Li, L.; Yuan, D.X. Spatial Variations of CO<sub>2</sub> Degassing Across Water-air Interface and Its Impact Factors in Summer in Guijiang River, China. *Environ. Sci.* **2017**, *38*, 11. (In Chinese)
23. Regnier, P.; Friedlingstein, P.; Ciais, P.; Thullner, M. Anthropogenic perturbation of the carbon fluxes from land to ocean. *Nat. Geosci.* **2013**, *6*, 597–607. [[CrossRef](#)]
24. Tranvik, L.J.; Downing, J.A.; Cotner, J.B.; Loiselle, S.A.; Striegl, R.G.; Ballatore, T.J.; Dillon, P.; Finlay, K.; Fortino, K.; Knoll, L.B.; et al. Lakes and reservoirs as regulators of carbon cycling and climate. *Limnol. Oceanogr.* **2009**, *54*, 2298–2314. [[CrossRef](#)]
25. Raymond, P.A.; Hartmann, J.; Lauerwald, R.; Sobek, S.; McDonald, C.; Hoover, M.; Butman, D.; Striegl, R.; Mayorga, E.; Humborg, C.; et al. Global carbon dioxide emissions from inland waters. *Erratum in Nature* **2014**, *503*, 355–359. [[CrossRef](#)]
26. Butman, D.; Raymond, P.A. Significant efflux of carbon dioxide from streams and rivers in the United States. *Nat. Geosci.* **2011**, *4*, 839–842. [[CrossRef](#)]
27. Pu, J.B.; Li, J.H.; Khadka, M.B.; Martin, J.B.; Zhang, T.; Yu, S.; Yuan, D.X. In-stream metabolism and atmospheric carbon sequestration in a groundwater-fed karst stream. *Sci. Total Environ.* **2017**, *579*, 1343–1355. [[CrossRef](#)]
28. Li, Y.J.; Zhang, H.T.; Xiao, J.; Qiu, X.L.; Wang, B.L. Effects of river hydrology on phytoplankton dynamics in dammed rivers. *Earth Environ.* **2019**, *47*, 857–863. (In Chinese)
29. Tan, S.C.; Shi, G.Y. Remote sensing for ocean primary productivity and its spatio-temporal variability in the China Seas. *Acta Geogr. Sin.* **2006**, *61*, 1189–1199.
30. Wang, J.Y. Comparison Table of Water Environment Monitoring Parameters and Selection Standards. *Water Conserv. Tech. Superv.* **2004**, *4*, 53–63. (In Chinese)

31. Zhang, T.; Li, J.H.; Pu, J.B.; Martin, J.B.; Khadka, M.B.; Wu, F.H.; Li, L.; Jiang, F.; Huang, S.Y.; Yuan, D.X. River sequesters atmospheric carbon and limits the CO<sub>2</sub> degassing in karst area, southwest China. *Sci. Total Environ.* **2017**, *609*, 92–101. [[CrossRef](#)] [[PubMed](#)]
32. Duchemin, E.; Lucotte, M.; Canuel, R.; Chamberland, A. Production of the greenhouse gases CH<sub>4</sub> and CO<sub>2</sub> by hydroelectric reservoirs of the boreal region. *Glob. Biogeochem. Cycles* **1995**, *9*, 529–540. [[CrossRef](#)]
33. Liu, J.; Xiao, S.B.; Wang, C.H.; Yang, Z.J.; Liu, D.F.; Guo, X.; Liu, L.; Lorke, A. Spatial and temporal variability of dissolved methane concentrations and diffusive emissions in the Three Gorges Reservoir. *Water Res.* **2021**, *207*, 117788. [[CrossRef](#)] [[PubMed](#)]
34. Zhang, T.; Li, J.H.; Pu, J.B.; Martin, J.B.; Yuan, D.X. Rainfall possibly disturbs the diurnal pattern of CO<sub>2</sub> degassing in the Lijiang River, SW China. *J. Hydrol.* **2020**, *590*, 125540. [[CrossRef](#)]
35. Odum, H.T. Primary Production in Flowing Waters. *Limnol. Oceanogr.* **1956**, *1*, 102–117. [[CrossRef](#)]
36. Doctor, D.H.; Kendall, C.; Sebestyen, S.D.; Shanley, J.B.; Ohte, N.; Boyer, E.W. Carbon isotope fractionation of dissolved inorganic carbon (DIC) due to outgassing of carbon dioxide from a headwater stream. *Hydrol. Process.* **2008**, *22*, 2410–2423. [[CrossRef](#)]
37. Wallin, M.; Audet, J.; Peacock, M.; Sahlee, E.; Winterdahl, M. Carbon dioxide dynamics in an agricultural headwater stream driven by hydrology and primary production. *Biogeosciences* **2020**, *17*, 2487–2498. [[CrossRef](#)]
38. Abril, G.L.; Guérin, F.; Richard, S.; Delmas, R.; Corinne, G.L.; Gosse, P.; Tremblay, A. Carbon dioxide and methane emissions and the carbon budget of a 10-year old tropical reservoir (Petit Saut, French Guiana). *Glob. Biogeochem. Cycles* **2005**, *19*, 4. [[CrossRef](#)]
39. Hotchkiss, E.R.; Hall, R.O.; Sponseller, R.A.; Butman, D.; Klaminder, J.; Laudon, H.; Rosvall, M.; Karlsson, J. Sources of and processes controlling CO<sub>2</sub> emissions change with the size of streams and rivers. *Nat. Geosci.* **2015**, *8*, 696. [[CrossRef](#)]
40. Yang, M.X.; Liu, Z.H.; Sun, H.L.; Yang, R.; Chen, B. Organic carbon source tracing and DIC fertilization effect in the Pearl River: Insights from lipid biomarker and geochemical analysis. *Appl. Geochem.* **2016**, *73*, 132–141. [[CrossRef](#)]
41. Wang, W.F.; Li, S.L.; Zhong, J.; Wang, L.C.; Yang, H.; Xiao, H.Y.; Liu, C.Q. CO<sub>2</sub> emissions from karst cascade hydropower reservoirs: Mechanisms and reservoir effect. *Environ. Res. Lett.* **2021**, *16*, 044013. [[CrossRef](#)]
42. de Montety, V.; Martin, J.B.; Cohen, M.J.; Foster, C.; Kurz, M.J. Influence of diel biogeochemical cycles on carbonate equilibrium in a karst river. *Chem. Geol.* **2011**, *283*, 31–43. [[CrossRef](#)]
43. Stumm, W.; Morgan, J.J. *Aquatic Chemistry: Chemical Equilibria and Rates in Natural Waters*, 3rd ed.; Wiley: Hoboken, NJ, USA, 1995; Volume 179, p. A277.
44. Marx, A.; Hintze, S.; Sanda, M.; Jankovec, J.; Barth, J.A. Acid rain footprint three decades after peak deposition: Long-term recovery from pollutant sulphate in the Uhlirska catchment (Czech Republic). *Sci. Total Environ.* **2017**, *598*, 1037–1049. [[CrossRef](#)]
45. Li, D.Y.; Zhang, L.K.; Li, C.F.; Wang, X.Y.; Wang, X.R.; Yang, Z.F.; Qian, L.T. Quantitative analysis of dissolved inorganic carbon sources in water bodies in the Lujiang River Basin. *Carsologica Sin.* 1–17. Available online: <https://link.cnki.net/urlid/45.1157.P.20231016.1203.002> (accessed on 16 October 2023). (In Chinese).
46. Zhang, L.K.; Qin, X.Q.; Yang, H.; Huang, Q.B.; Liu, P.Y. Characteristics of river carbon output flux and variation in the Pearl River Basin. *Environ. Sci.* **2013**, *34*, 10. (In Chinese) [[CrossRef](#)]
47. Dagg, M.; Benner, R.; Lohrenz, S.; Lawrence, D. Transformation of dissolved and particulate materials on continental shelves influenced by large rivers: Plume processes. *Cont. Shelf Res.* **2004**, *24*, 833–858. [[CrossRef](#)]
48. Kendall, C.; Silva, S.R.; Kelly, V.J. Carbon and nitrogen isotopic compositions of particulate organic matter in four large river systems across the United States. *Hydrol. Process.* **2010**, *15*, 7. [[CrossRef](#)]
49. LaZerte, B.D. Stable carbon isotope ratios: Implications for the source of sediment carbon and for phytoplankton carbon assimilation in Lake Memphremagog, Quebec. *Can. J. Fish. Aquat. Sci.* **1983**, *40*, 1658–1666. [[CrossRef](#)]
50. Hung, J.J.; Lin, L.L.; Liu, K.K. Dissolved and particulate organic carbon in the southern East China Sea. *Cont. Shelf Res.* **2000**, *20*, 4–5. [[CrossRef](#)]
51. Li, Z.K.; Lan, J.; Wang, G.; Han, B.; Lu, Y.F.; He, Q.; Zhang, Z.H. Mutual inductance measurement of the superconducting coil for Joule Balance. *IEEE Trans. Instrum. Meas.* **2013**, *62*, 1531–1536. [[CrossRef](#)]
52. Raymond, P.A.; Bauer, J.E.; Caraco, N.F.; Cole, J.J.; Longworth, B.; Petsch, S.T. Controls on the variability of organic matter and dissolved inorganic carbon ages in northeast US rivers. *Mar. Chem.* **2004**, *92*, 353–366. [[CrossRef](#)]
53. Teodoru, C.R.; Giorgio, P.A.; Prairie, Y.T.; Camire, M. Patterns in pCO<sub>2</sub> in boreal streams and rivers of northern Quebec, Canada. *Glob. Biogeochem. Cycles* **2009**, *23*, GB2012. [[CrossRef](#)]
54. Varol, M.; Li, S.Y. Biotic and abiotic controls on CO<sub>2</sub> partial pressure and CO<sub>2</sub> emission in the Tigris River, Turkey. *Chem. Geol.* **2017**, *449*, 193. [[CrossRef](#)]
55. Yao, G.R.; Gao, Q.Z.; Wang, Z.G.; Huang, X.K.; He, T.; Zhang, Y.L.; Jiao, S.L.; Ding, J. Dynamics of CO<sub>2</sub> partial pressure and CO<sub>2</sub> outgassing in the lower reaches of the Xijiang River, a subtropical monsoon river in China. *Sci. Total Environ.* **2007**, *376*, 255–266. [[CrossRef](#)] [[PubMed](#)]
56. Alin, S.R.; Rasera, M.L.; Salimon, C.I.; Richey, J.E.; Holtgrieve, G.W.; Krusche, A.V.; Snidvongs, A. Physical controls on carbon dioxide transfer velocity and flux in low-gradient river systems and implications for regional carbon budgets. *J. Geophys. Res. Biogeosciences* **2011**, *116*, g01009. [[CrossRef](#)]
57. Li, S.Y.; Lu, X.X.; Bush, R.T. CO<sub>2</sub> partial pressure and CO<sub>2</sub> emission in the Lower Mekong River. *J. Hydrol.* **2013**, *504*, 40–56. [[CrossRef](#)]
58. Rocher-Ros, G.; Harms, T.K.; Sponseller, R.A.; Visnen, M.; Mrth, C.; Giesler, R. Metabolism overrides photo-oxidation in CO<sub>2</sub> dynamics of Arctic permafrost streams. *Limnol. Oceanogr.* **2020**, *66*, S169–S181. [[CrossRef](#)]

59. Louis, V.S.; Kelly, C.A.; Duchemin, E.; Rudd, J.W.; Rosenberg, D.M. Reservoir surfaces as sources of greenhouse gases to the atmosphere: A global estimate. *Bioscience* **2000**, *50*, 766–775. [[CrossRef](#)]
60. TERNON, J.F.; OUDOT, C.; DESSIER, A.; DIVERRES, D. A seasonal tropical sink for atmospheric CO<sub>2</sub> in the Atlantic ocean: The role of the Amazon River discharge. *Mar. Chem.* **2000**, *68*, 183–201. [[CrossRef](#)]
61. Yang, C.; Telmer, K.; Veizer, J. Chemical dynamics of the “St. Lawrence” riverine system:  $\delta D_{H_2O}$ ,  $\delta^{18}O_{H_2O}$ ,  $\delta^{13}C_{DIC}$ ,  $\delta^{34}S$  sulfate, and dissolved  $^{87}Sr/^{86}Sr$ . *Geochim. Et Cosmochim. Acta* **1996**, *60*, 851–866. [[CrossRef](#)]
62. Raymond, P.A.; Bauer, J.E.; Cole, J.J. Atmospheric CO<sub>2</sub> evasion, dissolved inorganic carbon production, and net heterotrophy in the York River estuary. *Limnol. Oceanogr.* **2000**, *45*, 1707–1717. [[CrossRef](#)]
63. Santos, M.A.; Rosa, L.P.; Sikar, B.; Sikar, E.; Santos, E.O. Gross greenhouse gas fluxes from hydro-power reservoir compared to thermo-power plants. *Energy Policy* **2006**, *34*, 481–488. [[CrossRef](#)]
64. Liu, C.Q.; Wang, F.S.; Wang, Y.C.; Wang, B.L. Responses of Aquatic Environment to River Damming—From the Geochemical View. *Resour. Environ. Yangtze Basin* **2009**, *18*, 384–396.
65. Yu, Y.X.; Liu, C.Q.; Wang, F.S.; Wang, B.L.; Liu, F. Spatiotemporal characteristics and diffusion flux of partial pressure of dissolved carbon dioxide ( $pCO_2$ ) in Hongjiadu reservoir. *Chin. J. Ecol.* **2008**, *27*, 1193–1199.
66. Mei, H.Y.; Wang, F.S.; Yao, C.C.; Wang, B.L. Diffusion flux of partial pressure of dissolved carbon dioxide in Wan’an Reservoir in spring. *Environ. Sci.* **2011**, *32*, 58–63.

**Disclaimer/Publisher’s Note:** The statements, opinions and data contained in all publications are solely those of the individual author(s) and contributor(s) and not of MDPI and/or the editor(s). MDPI and/or the editor(s) disclaim responsibility for any injury to people or property resulting from any ideas, methods, instructions or products referred to in the content.